Calculations of Spectroscopic Properties of the LH2 Bacteriochlorophyll−Protein Antenna Complex from *Rhodopseudomonas acidophila*†

R. G. Alden,‡ E. Johnson, V. Nagarajan, and W. W. Parson*

Department of Biochemistry, Box 357350, University of Washington, Seattle, Washington 98195-7350

C. J. Law and R. G. Cogdell

Division of Biochemistry and Molecular Biology, University of Glasgow, Glasgow G12 8QQ, U.K.

Received: December 17, 1996; In Final Form: March 5, 1997⊗

Absorption and CD spectra of a photosynthetic bacterial antenna complex are calculated on the basis of the crystal structure of the LH2 (B800-850) complex from *Rhodopseudomonas acidophila.* This complex contains a ring of 18 tightly coupled bacteriochlorophylls (B850) and a ring of 9 more weakly coupled bacteriochlorophylls (B800). Molecular orbitals for bacteriochlorophylls with the three different geometries seen in the crystal structure are obtained by semiempirical quantum mechanical calculations (QCFF/PI). Exciton and charge-transfer interactions are introduced at the level of configuration interactions. Particular attention is paid to the dependence of these interactions on the interatomic distances and on dielectric screening. Absorption band shapes are treated with the aid of vibronic parameters and homogeneous line widths that have been measured by hole burning (Reddy, N. R. S., et al., *Photochem. Photobiol.* **1993**, *57*, 35−39). Inhomogeneous broadening due to diagonal disorder in the monomeric and charge-transfer transition energies is included by a Monte Carlo method. The calculations successfully reproduce the main features of measured absorption and CD spectra of the complex. The results support the view that the excited states of the B850 bacteriochlorophylls are extensively delocalized over the ring of pigments while the excited states of the B800 bacteriochlorophylls are much more localized.

The light-harvesting (LH) antenna systems of photosynthetic bacteria and plants transfer excitation energy rapidly to the photosynthetic reaction centers, where the energy is trapped in an electron-transfer reaction.[1−3] Photosynthetic bacteria contain two major types of antenna complexes. One of these (LH1 or B875) is believed to surround the reaction centers, while the other (LH2 or B800-850) forms a peripheral network of pigment−protein complexes, each of which holds between 20 and 30 molecules of bacteriochlorophyll (BChl). The recent solution of crystal structures of LH2 complexes from *Rhodopseudomonas acidophila*[4] and *Rhodospirillum molischianum*[5] has opened the door to an increasingly detailed understanding of the unusual spectroscopic and dynamic properties of the bacterial antenna complexes.

The LH2 complex from *Rp. acidophila* strain 10050 consists of nine copies of each of two proteins (α and *β*), 27 BChl-*a* molecules, and 18 carotenoids, arranged in a cylindrical structure with C_9 crystallographic symmetry.[4] The pigments form an inner ring of 18 BChls with a center-to-center distance of about 9 Å and an outer ring of 9 BChls with center-to-center distances of about 21 Å. The two rings are offset by 16.5 Å along the cylinder axis. The normals to the molecular planes of the BChls in the inner ring are aligned approximately perpendicular to the symmetry axis, whereas those of BChls in the outer ring are approximately parallel to this axis. Figure 1 shows the structure of the repeating unit of two BChls in the inner ring and one in the outer. One of the BChls in the inner ring is noticeably distorted from planarity.[2]

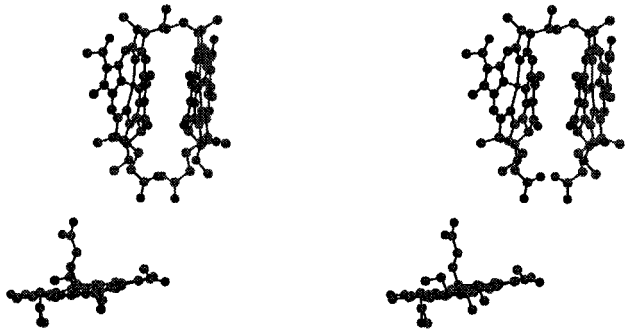

Figure 1. Stereoview of the three BChl-*a* molecules in the asymmetric unit of the LH2 complex of *Rp. acidophila*, from a perspective approximately perpendicular to the C_9 symmetry axis. A B850 BChl bound to an α polypeptide is at the top right, a B850 BChl bound to a *β* polypeptide at the top left, and a B800 BChl at the bottom.

The absorption spectra of LH2 complexes from *Rp. acidophila* and other related bacterial species differ substantially from the spectrum of monomeric BChl in solution. The long-wavelength (Q_y) absorption band of monomeric BChl-*a in vitro* occurs at 770−780 nm and has negligible rotational strength. LH2 complexes have two strong absorption bands in the near IR, one in the region of 850−860 nm and the other near 800 nm (Figure 2A). The long-wavelength absorption band of the LH2 complex of *Rp. acidophila* occurs at 859 nm at room temperature and at 870 nm at 4 K.[6] The CD spectrum (Figure 2B) displays a negative lobe on the red side of the long-wavelength absorption band, a positive lobe on the blue side of this band, and a somewhat weaker pair of lobes with reversed signs on either side of the 800-nm band.

† *Abbreviations*: BChl, bacteriochlorophyll; CD, circular dichroism; CI, configuration interaction; CT, charge transfer; fwhm, full width at half-maximal amplitude; LH, light-harvesting; QCFF/PI, quantum mechanical consistent force field/*π*-electron.

* Corresponding author.

‡ Current address: NC Applications Division, Boeing, Everett, WA 98203.

⊗ Abstract published in *Advance ACS Abstracts,* May 15, 1997.

S1089-5647(97)00005-9 CCC: $14.00

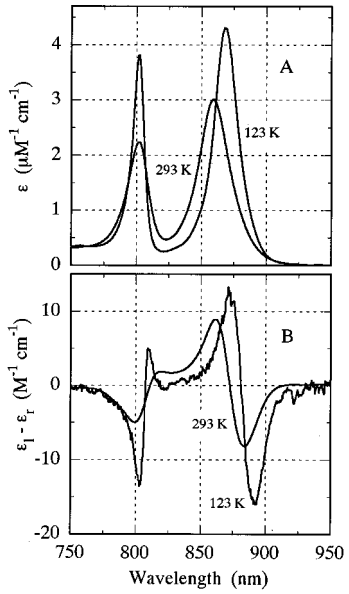

Figure 2. Measured absorption (A) and CD (*B*) spectra of purified *Rp. acidophila* LH2 complexes suspended in 40% (20 mM Tris HCl, pH 8.0, 0.1% lauryldimethylamine oxide) 60% glycerol at 293 and 123 K. A linear base line was subtracted to set the CD to zero at 700 and 950 nm. Note that the units of the absorbance and CD scales differ by a factor of 10^6. The experimental uncertainties in ϵ and $\epsilon_l - \epsilon_r$ are approximately ±10%.

The crystal structure of the LH2 complex suggests that the 18 closely spaced and, presumably, strongly coupled BChls give rise to the absorption band in the 850-nm region, while the outer, more weakly coupled BChls are responsible for the absorption band at 800 nm.[2,7] This supposition is in accord with the larger dipole strength of the 860-nm band and with measurements of linear dichroism.[8] The BChls in the inner and outer rings have therefore been termed the "B850" and "B800" BChls, respectively. Fluorescence emission occurs mainly to the red of the B850 band, but the fluorescence excitation spectrum exhibits a strong component at 800 nm as well as at 850 nm, indicative of efficient energy transfer from B800 to B850.[9] Time-resolved measurements have shown that, in the similar complex from *Rhodobacter sphaeroides*, the transfer occurs with a time constant of about 0.7 ps at 295 K.[10−12]

A knowledge of the electronic states that give rise to the absorption and emission spectra of the LH2 complex is critical to a detailed understanding of the mechanism of energy transfer. The most practical way to approach a system of this size probably is to use a semiempirical quantum mechanical method such as the quantum-mechanical-consistent-force-field/π-electron (QCFF/PI) method[13,14] to treat the individual BChl molecules and to introduce intermolecular interactions at the level of configuration interactions (CI). Warshel and Parson[15,16] used this strategy to explore the spectroscopic properties of the reaction center of *Rhodopseudomonas viridis*. Their treatment included charge-transfer (CT) states explicitly and used transition monopoles rather than point dipoles to evaluate exciton interactions. The same approach later was used to treat oxidized reaction centers[17] and crystalline methylbacteriopheophorbide-*a*.[18] Sauer et al.[7] recently described similar calculations that reproduced some of the spectroscopic properties of the *Rp. acidophila* LH2 complex. To account for the energy of the long-wavelength absorption band, it appeared necessary to lower the monomer transition energies assigned to the B850 BChls by about 240 cm^{-1} relative to the energies of the B800 BChls. Although the calculated CD spectrum did not match the measured spectrum well, bands with positive and negative rotational strengths were obtained in the correct regions. In these calculations, the same molecular orbitals were used for all the BChls. Mixing of the Q_y transitions with CT, Q_x, and Soret transitions was not included explicitly, and absorption line shapes were introduced by dressing the calculated stick spectra with Gaussians.

In the present work, the QCFF/PI-CI approach is used to calculate the absorption and CD spectra of the LH2 complex of *Rp. acidophila*. We have refined the treatment of the distance dependences of intermolecular exciton and CT interactions, used different molecular orbitals and transition energies for BChls with the three geometries seen in the crystal structure, included inhomogeneous distributions of monomer transition energies, and used a realistic treatment of the absorption line shapes based on experimentally measured vibronic parameters and homogeneous line widths. We focus particularly on the question of whether the main excited states of the LH2 complex are extensively delocalized over the chromophore rings or are localized on smaller groups of pigments.

Methods

Monomer Wave Functions and Spectroscopic Properties. The wave functions for isolated BChl molecules were obtained by the QCFF/PI method using the heteroatom parameters from Table 4 of Warshel and Lapicirella.[14] Molecular π-orbitals for the individual molecules are written as linear combinations of atomic orbitals

$$\phi_n^s = \sum_t \nu_{n,t}^s \chi_t^s \tag{1}$$

where χ_t^s is an atomic 2pπ orbital on atom t of molecule s, and the expansion coefficients ($\nu_{n,t}^s$) are obtained by solving the self-consistent field equation.[13] The major optical absorption bands of BChl are due to transitions involving the top two filled molecular orbitals and the two lowest unfilled orbitals.[19,20] We will denote this set of orbitals for molecule s by ϕ_1^s to ϕ_4^s in order of increasing energy. Separate sets of orbitals were generated for BChl molecules in each of the three different geometries found in the LH2 crystal structure (see Figure 1). The coefficients obtained for the three structures are given in the Supporting Information. In the present study, we did not consider perturbations of the orbitals by hydrogen bonding or electrostatic interactions with the protein.

Wave functions for the excited states of an individual BChl can be written as

$$\Psi_i^s = \sum_N c_{i,N}^s \, {}^1\Psi_N^s \tag{2}$$

where ${}^1\Psi_N^s$ is the Slater determinant corresponding to a singlet excitation from orbital ϕ_{n1}^s to ϕ_{n2}^s (${}^1\Psi_N^s \equiv {}^1\Psi_{n1\rightarrow n2}^s$) and the $c_{i,N}^s$ are intramolecular CI coefficients. In the four-orbital model this treatment yields four excited states termed Q_y, Q_x, B_y and B_x.[15] The Q_y and B_y transitions are due primarily to excitations from ϕ_2 to ϕ_3 and from ϕ_1 to ϕ_4; the Q_x and B_x transitions, to excitations from ϕ_2 to ϕ_4 and from ϕ_1 to ϕ_3. The calculated Q_y excitation energies varied significantly for molecules with the three different geometries in the crystal structure. Relative to B800, the energy for B850-α was lower by 216 cm^{-1} and that for B850-β (which has the largest departure from planarity) was lower by 307 cm^{-1}. Jentzen et al.[21] and Barkigia et al.[22] have described similar variations in calculated Q_y excitation energies with structural distortions in BChl and other related molecules.

Transition dipoles for the intramolecular excitations ($\vec{\mu}_i^s$) were calculated using the "transition gradient" or "dipole velocity" representation:

$$\vec{\mu}_i^s \approx (e\hbar\sqrt{2}/2\pi mc\bar{\nu}_i^s)\sum_N c_{i,N}^s \sum_{t1}\sum_{t2} \nu_{n1,t1}^s \nu_{n2,t2}^s \langle\chi_{t2}^s|\tilde{\nabla}|\chi_{t1}^s\rangle = (e\hbar\sqrt{2}/2\pi mc\bar{\nu}_i^s)\sum_N c_{i,N}^s \sum_{t1}\sum_{t2>t1} (\nu_{n1,t1}^s \nu_{n2,t2}^s - \nu_{n1,t2}^s \nu_{n2,t1}^s)\langle\chi_{t2}^s|\tilde{\nabla}|\chi_{t1}^s\rangle \quad (3)$$

where $\bar{\nu}_i^s$ is the energy of transition i of molecule s, $\tilde{\nabla} = (\partial/\partial x, \partial/\partial y, \partial/\partial z)$, e and m are the electron charge and mass, and c is the speed of light. Here, and for all the subsequent calculations, we set $\bar{\nu}_i^s$ at 12 500 cm^{-1} for the Q_y transition of BChl with the B800 geometry, corresponding to a wavelength of 800 nm. We reduced the energies for B850-α and B850-β to 12 284 and 12 193 cm^{-1}, respectively, in accord with the calculated energy differences between the three structures. The Q_x, B_x and B_y transitions were assigned energies of 16 667, 24 390 and 27 027 cm^{-1}, respectively, for all three structures.

The terms in eq 3 were evaluated for all intramolecular atom pairs ($t1$, $t2$) with interatomic distances less than 20 Å, although decreasing the cutoff distance to 5 Å had little effect on the results. To take into account the distortions of the BChl molecules from planarity, the individual interatomic matrix elements were calculated from the expression

$$\langle\chi_{t2}^s|\tilde{\nabla}|\chi_{t1}^s\rangle = (\eta_{x,t1}\eta_{y,t2} + \eta_{y,t1}\eta_{x,t2})\nabla_{xy}\hat{\imath} + [\eta_{y,t1}\eta_{y,t2}\nabla_\sigma + (\eta_{x,t1}\eta_{x,t2} + \eta_{z,t1}\eta_{z,t2})\nabla_\pi]\hat{\jmath} + (\eta_{z,t1}\eta_{y,t2} + \eta_{y,t1}\eta_{z,t2})\nabla_{xy}\hat{k} \quad (4)$$

Here $\eta_{x,t}$, $\eta_{y,t}$, and $\eta_{z,t}$ are direction cosines of the $2p\pi$ orbital on atom t (χ_t^s) with respect to a Cartesian coordinate system (x, y, z) defined so that the y axis is along the line from atom $t1$ to $t2$; $\hat{\imath}$, $\hat{\jmath}$, and $\hat{k}$ are unit vectors in this system, and ∇_σ, ∇_π, and ∇_{xy} are the matrix elements of $\tilde{\nabla}$ for pairs of Slater-type 2p orbitals in canonical orientations and at the appropriate interatomic distance. ∇_π is for two p_x or p_z orbitals; ∇_σ, for two p_y orbitals; ∇_{xy}, for p_x and p_y orbitals. ($\nabla_{zy} = \nabla_{xy}$ and $\nabla_{xz} = 0$.) The dependences of ∇_σ, ∇_π, and ∇_{xy} on the interatomic distance and the Slater orbital parameter ζ for C, N, and O atoms were evaluated as described in Appendix A.

The CI coefficients ($c_{i,N}^s$) for the intramolecular transitions were adjusted to optimize the agreement between the dipole strengths ($|\vec{\mu}_i^s|^2$) calculated with eq 3 and those measured experimentally for monomeric BChl-*a* in solution. A dipole strength of 50 D^2 (D = 1 debye) was used for the Q_y transitions, and 19 D^2 for Q_x (see Appendix B). Because the B_y and B_x transitions are not well resolved in the absorption spectra, we did not attempt to refine the $c_{i,N}^s$ for these transitions independently, but rather used the values obtained by a symmetry transformation of the Q_y and Q_x coefficients.[15] Separate sets of CI coefficients were obtained for BChl molecules with the three different geometries in the crystal structure (Figure 1), on the assumption that the dipole strengths are the same for all three geometries. The optimized coefficients are given in the Supporting Information. Although the actual dipole strengths undoubtedly vary somewhat, the differences between the CI coefficients obtained for the three structures are small and have little effect on the results presented below. Note that our adjustment of the CI coefficients is part of the initial parameterization of the wave functions of monomeric BChl and does not represent an empirical fitting of spectroscopic data on the LH2 complex.

Molecular magnetic transition dipoles also were calculated with the gradient representation:

$$\vec{m}_i^s \approx (-e\hbar i\sqrt{2}/2\pi mc)\sum_N c_{i,N}^s \sum_{t1}\sum_{t2} \nu_{n1,t1}^s \nu_{n2,t2}^s \langle\chi_{t2}^s|\vec{r}\times\tilde{\nabla}|\chi_{t1}^s\rangle$$

$$\approx (-e\hbar i\sqrt{2}/2\pi mc)\sum_N c_{i,N}^s \sum_{t1}\sum_{t2>t1} (\nu_{n1,t1}^s \nu_{n2,t2}^s - \nu_{n1,t2}^s \nu_{n2,t1}^s)\vec{r}_{t1,t2}^{\,o} \times \langle\chi_{t2}^s|\tilde{\nabla}|\chi_{t1}^s\rangle \quad (5)$$

where $\vec{r}_{t1,t2}^{\,o}$ is the vector from the origin of the coordinate system to the point midway between atoms $t1$ and $t2$.

Oligomer Wave Functions. Interactions between the BChls in an oligomeric structure can be introduced by writing a CI matrix for the excited states of the system:

$$\mathbf{U} = \begin{bmatrix} [\mathbf{U}^{loc}] & [\mathbf{U}^{loc,CT}] \\ [\mathbf{U}^{CT,loc}] & [\mathbf{U}^{CT}] \end{bmatrix} \quad (6)$$

The excitation energies of the intramolecular or "local" transitions (Q_y, Q_x, B_y and B_x) of the individual BChls appear as diagonal terms in the upper left-hand block of $\mathbf{U}$ ($\mathbf{U}^{loc}$). The off-diagonal terms in this block represent exciton interactions between the transitions of separate molecules. In the lower right-hand block ($\mathbf{U}^{CT}$), the diagonal terms are the energies of intermolecular charge-transfer transitions, and the off-diagonal terms represent mixing of different CT transitions. The $\mathbf{U}^{CT,loc}$ and $\mathbf{U}^{loc,CT}$ blocks describe the mixing of local and CT transitions. In the B800-B850 complex of *Rp. acidophila* each of the 27 BChl monomers has four possible singlet excitations, giving a total of 108 local excited states. Although we will be concerned mainly with absorption bands in the near IR, which depend primarily on the Q_y transitions, it is important in principle to retain the higher-energy transitions as well because of their possible contributions to hyperchromism or hypochromism of the long-wavelength bands.[23] In addition to the local transitions, each pair of BChls has eight possible CT transitions (an electron originating in either ϕ_1^{s1} or ϕ_2^{s1} of BChl $s1$ can move to either ϕ_3^{s2} or ϕ_4^{s2} of BChl $s2$, and an electron originating in ϕ_1^{s2} or ϕ_2^{s2} can move to ϕ_3^{s1} or ϕ_4^{s1}). Again, although only the $\phi_2 \rightarrow \phi_3$ CT transitions are expected to make significant contributions to the near-IR absorption bands, we retained the higher-energy CT transitions for consistency. The CT transitions have no intrinsic dipole strength but contribute to the absorption and CD spectra to the extent that they mix with the intramolecular transitions. Because the matrix elements that control this mixing ($\mathbf{U}^{CT,loc}$ and $\mathbf{U}^{loc,CT}$) drop off very rapidly with distance (see below), it is sufficient to consider CT interactions only between neighboring molecules in the ring of B850 BChls. This restriction reduces the number of CT transitions to 144 (8 × 18). The total size of $\mathbf{U}$ is, therefore, 252 × 252.

The exciton-interaction matrix element that mixes local transition i of one BChl with transition k of another can be expanded with the transition-monopole expression

$$\mathbf{U}_{i(s1),k(s2)}^{loc} = 2\Omega_{i(s1),k(s2)}\sum_N c_{i,N}^{s1}\sum_{t1}\nu_{n1,t1}^{s1}\nu_{n2,t1}^{s1}\sum_M c_{k,M}^{s2}\sum_{t2}\nu_{m1,t2}^{s2}\nu_{m2,t2}^{s2}\gamma_{t1,t2}/d_{t1,t2} \quad (7)$$

where $\gamma_{t1,t2}$ is the electron−electron repulsion integral between $2p\pi$ electrons on atom $t1$ of BChl $s1$ and atom $t2$ of BChl $s2$, $d_{t1,t2}$ is a dielectric screening factor, and $\Omega_{i(1),k(2)}$ is a factor that corrects for imperfections in the molecular orbitals (see below).

To evaluate the repulsion integrals, we used the two-center integrals originally derived by Roothaan.[24] The Roothaan integrals for pairs of 2p orbitals in canonical orientations and at the appropriate interatomic distances (R_σ, R_π, R_{xz}, and R_{xy}) were weighted by products of direction cosines in a manner analogous to that described above for the intramolecular gradient integrals:

$$\gamma_{t1,t2} = (\eta_{y,t1}\eta_{y,t2})^2 R_\sigma + [(\eta_{x,t1}\eta_{x,t2} + \eta_{z,t1}\eta_{z,t2})^2]R_\pi + [(\eta_{x,t1}\eta_{z,t2})^2 + (\eta_{z,t1}\eta_{x,t2})^2]R_{xz} + [(\eta_{x,t1}\eta_{y,t2})^2 + (\eta_{y,t1}\eta_{x,t2})^2 + (\eta_{z,t2}\eta_{y,t1})^2 + (\eta_{y,t2}\eta_{z,t1})^2]R_{xy} \quad (8)$$

At interatomic distances beyond about 6 Å, values for the repulsion integrals calculated in this way are essentially identical to those obtained with the simpler expression used in previous calculations on reaction centers.[15] At shorter distances, the Roothaan integrals probably capture more accurately the dependence on the relative orientations of the two orbitals. However, this has only minor effects on the calculated spectroscopic properties of the LH2 complex.

The dielectric screening factor in eq 7 represents the effects of high-frequency induced dipoles in the protein and solvent. At large interatomic distances, $d_{t1,t2}$ should be approximately n^2, where n is the refractive index of the protein; at short distances, $d_{t1,t2}$ should approach 1. We therefore used a distance-dependent screening factor:

$$d_{t1,t2} = n^2 + (1 - n^2)e^{-(r_{t1,t2}/r_o)^3} \quad (9)$$

where $r_{t1,t2}$ is the distance between atoms $t1$ and $t2$, $n^2 = 2$, and r_o is an adjustable parameter on the order of 4 Å.[25] The dependence of the results on the choice of r_o is discussed below.

The correction factor $\Omega_{i(s1),k(s2)}$ is given by

$$\Omega_{i(s1),k(s2)} = [(D^{\nabla}_{i(s1)}/D^{R}_{i(s1)})(D^{\nabla}_{k(s2)}/D^{R}_{k(s2)})]^{1/2} \quad (10)$$

Here $D^{\nabla}_{i(s1)}$ and $D^{\nabla}_{k(s2)}$ are the dipole strengths calculated by eq 3 for transition i and k of monomeric BChls $s1$ and $s2$, respectively, and $D^{R}_{i(s1)}$ and $D^{R}_{k(s2)}$ are the dipole strengths calculated using the dipole operator (*i.e.*, with $\vec{r}$ replacing $\tilde{\nabla}$ and $\sqrt{2}e$ replacing the factor $e\hbar\sqrt{2}/2\pi mc\bar{\nu}^s_i$). This correction has been used in calculations of excimer fluorescence of polycyclic aromatic molecules[26,27] and in previous calculations on reaction centers.[15-17] The magnitude of $\Omega_{i(s1),k(s2)}$ for BChl Q_y transitions is typically about 0.5.

We now turn to the portions of **U** that involve CT transitions. For a transition from orbital $n1$ of BChl $s1$ to $n2$ of BChl $s2$ ($\phi^{s1}_{n1} \rightarrow \phi^{s2}_{n2}$), the CT energy that constitutes one of the diagonal elements of $\mathbf{U}^{CT}$ can be written

$$\mathbf{U}^{CT}_{n1(s1)\rightarrow n2(s2),n1(s1)\rightarrow n2(s2)} = \Delta E^{gas} + \Delta V^{QQ} + \Delta V^{sol} \quad (11)$$

where ΔE^{gas} is the gas-phase energy difference between orbitals $n1$ and $n2$ ($E^{s2}_{n2} - E^{s1}_{n1}$), ΔV^{QQ} is the change in charge−charge interactions between the two BChls (without dielectric screening), and ΔV^{sol} represents the change in electrostatic interactions with the partial charges and induced dipoles of the protein and solvent atoms. Because the model used in the present study did not include the protein and solvent explicitly, ΔV^{sol} could not be evaluated microscopically. We therefore used eq 11 only to estimate the relative energies of the eight CT transitions in which an electron moves from one to the other of a given pair of BChls and of corresponding transitions involving BChls in different positions. ΔV^{sol} was assumed to be the same for all the CT states, and the relative CT energies were calculated simply from the sum of ΔE^{gas} and ΔV^{QQ} with

$$\Delta V^{QQ} = \sum_{t1}(\nu^{s1}_{n1,t1})^2 \sum_{t1}(\nu^{s2}_{n2,t2})^2 \gamma_{t1,t2} \quad (12)$$

TABLE 1: Relative B850 Charge-Transfer Energies[a]

transition[b]	ΔE^{gas}	$\Delta E^{gas} + \Delta V^{QQ}$	
		1−1[c]	1−2[d]
$\alpha\phi_2 \rightarrow \beta\phi_3$	(0)	950	(0)
$\alpha\phi_1 \rightarrow \beta\phi_3$	4 050	4 300	4 250
$\alpha\phi_2 \rightarrow \beta\phi_4$	14 250	14 250	14 500
$\alpha\phi_1 \rightarrow \beta\phi_4$	18 300	18 300	18 750
$\beta\phi_2 \rightarrow \alpha\phi_3$	1 000	1 750	1 150
$\beta\phi_1 \rightarrow \alpha\phi_3$	4 900	5 150	5 100
$\beta\phi_2 \rightarrow \alpha\phi_4$	14 150	14 800	14 300
$\beta\phi_1 \rightarrow \alpha\phi_4$	18 000	18 150	18 500

[a] Energies are given in cm^{-1} relative to the energy of the $\alpha\phi_2 \rightarrow \beta\phi_3$ transition between adjacent $\alpha\beta$ B850 dimers. [b] B850 BChl types and orbitals. [c] Transitions within an individual $\alpha\beta$ B850 dimer. [d] Transitions between adjacent $\alpha\beta$ B850 dimers. ΔE^{gas} is the same for intra- and interdimer transitions.

Table 1 lists the relative energies of the various transitions. The lowest CT transition is transfer of an electron from ϕ_2 of a B850α BChl to ϕ_3 of the B850β BChl in the neighboring dimer. The energy for transferring an electron within an $\alpha\beta$ dimer is calculated to be higher by about 950 cm^{-1}. To examine how CT transitions affect the calculated spectroscopic properties, all of the CT transitions were moved up or down in energy together by adding an adjustable constant to the relative energies given in the third and fourth columns of the table.

The off-diagonal terms that mix two CT transitions in the same direction are given by

$$U^{CT}_{n1(s1)\rightarrow n2(s2),m1(s1)\rightarrow m2(s2)} = -\sum_{t1}\nu^{s1}_{n1,t1}\nu^{s1}_{m1,t1}\sum_{t2}\nu^{s2}_{n2,t2}\nu^{s2}_{m2,t2}\gamma_{t1,t2}/d_{t1,t2} \quad (13)$$

The corresponding terms for CT transitions in opposite directions are zero.[15]

The terms of the $\mathbf{U}^{loc,CT}$ submatrix, which describe interactions between local and CT transitions, are

$$U^{loc,CT}_{i(s1),m1(s1)\rightarrow m2(s2)} = \sum_N c^{s1}_{i,N}\delta_{n1,m1}\sum_{t1}\nu^{s1}_{n2,t1}\sum_{t2}\nu^{s2}_{m2,t2}\beta_{t1,t2}$$

$$U^{loc,CT}_{i(s2),m1(s1)\rightarrow m2(s2)} = -\sum_N c^{s2}_{i,N}\delta_{n2,m2}\sum_{t1}\nu^{s1}_{m1,t1}\sum_{t2}\nu^{s2}_{n2,t2}\beta_{t1,t2} \quad (14)$$

where $\beta_{t1,t2}$ is the atomic resonance integral for electrons on atoms $t1$ and $t2$. $\beta_{t1,t2}$ can be evaluated by resolving it into σ and π components:

$$\beta_{t1,t2} \approx \eta_{y,t1}\eta_{y,t2}\beta_\sigma + (\eta_{x,t1}\eta_{x,t2} + \eta_{z,t1}\eta_{z,t2})\beta_\pi \quad (15)$$

Semiempirical expressions for the σ and π resonance integrals β_σ and β_π as functions of interatomic distance $r_{t1,t2}$ have been given previously:[13,15]

$$\beta_\sigma = \exp(-2.7\rho/2)(8.51 \times 10^4 + 4.26 \times 10^4\rho + 4.26 \times 10^3\rho^2 - 1.42 \times 10^3\rho^3 - 3.55 \times 10^2\rho^4) \quad (16a)$$

and

$$\beta_\pi = 3.11 \times 10^5 \exp(-1.95 r_{t1,t2}) \quad (16b)$$

where $r_{t1,t2}$ is in Å, β_σ and β_π are in cm^{-1}, and $\rho = 5.385 r_{t1,t2}$.

However, these expressions are parameterized reliably only for short distances and probably underestimate the resonance integrals for longer distances in condensed media.[28−31] We therefore used the expressions

$$\beta_\sigma = -2.73 \times 10^6 \exp(-1.95 r_{t1,t2}) - 1.81 \times 10^4 \exp(-0.7 r_{t1,t2}) \quad (17a)$$

and

$$\beta_\pi = 2.80 \times 10^5 \exp(-1.95 r_{t1,t2}) + 3.89 \times 10^2 \exp(-0.7 r_{t1,t2}) \quad (17b)$$

The second term on the right in eq 17a was chosen to fit experimental data on the kinetics of long-range electron-transfer reactions in proteins.[32] The exponent and coefficient of the first term on the right in 17a were optimized by holding the second term constant and fitting the biexponential expression to eq 16a in the range $3.0 \le r_{t1,t2} \le 4.0$. Equation 17b was obtained by adding a term with an exponent of $-0.7 r_{t1,t2}$ to eq 16b. The coefficients of the two exponentials here were adjusted so that the ratio of the values of β_π given by eqs 17b and 16b at 4.0 Å was the same as the ratio of the values of β_σ given by 17a and 16a. Equations 17a and b are not intended to be used for $r_{t1,t2} < 3.0$.

The excited states of the LH2 complex now can be written

$$\vartheta_j = \sum_i C_i^j \varphi_i \quad (18)$$

where the φ_i are the 252 basis transitions. The coefficients C_i^j and the excitation energies are obtained by diagonalizing **U**.

The zero-order wave function for the ground state is

$$\vartheta_o = \prod_s \Psi_o^s \quad (19)$$

where Ψ_o^s is the ground state of molecule s. ϑ_o can mix with doubly-excited states in which two different BChls are both in excited singlet states. Considering 4 singly-excited states of each molecule, a complex of S BChls has $8S(S-1)$ doubly-excited states, or 5616 in the present case. Their individual contributions to the ground state are small and can be obtained from the terms of $\mathbf{U}^{\mathrm{loc}}$.[33] The coefficient for the state in which molecules $s1$ and $s2$ are in excited states i and k is

$$G_{i(s1),k(s2)} \approx -[U^{\mathrm{loc}}_{i(s1),k(s2)}/(\bar{\nu}_i^{s1} + \bar{\nu}_k^{s2})] G_o \quad (20)$$

where

$$G_o = \{1 + \sum_{s1} \sum_i \sum_{s2} \sum_k [U^{\mathrm{loc}}_{i(s1),k(s2)}/(\bar{\nu}^{s1}{}_i + \bar{\nu}_k^{s2})]^2\}^{-1/2} \quad (s1 \neq s2) \quad (21)$$

The small lowering of the ground-state energy was neglected.

Absorption and CD Spectra of the Complex. Transition dipoles for excitation of the LH2 complex to state ϑ_i are obtained by summing the transition dipoles of the individual molecules, weighting the contribution of each local transition by coefficient C_i^j, and including the contributions from downward transitions of the doubly excited states that are part of the ground state. The electric and magnetic transition dipoles are

$$\vec{\mu}_j^T = \sum_{s1} \sum_i \left\{ G_o C^j_{i(s1)} + \sum_{s2} G_{i(s1),k(s2)} C^j_{k(s2)} \right\} \vec{\mu}_i \quad (22)$$

$$\vec{m}_j^T = \sum_{s1} \sum_i \left\{ G_o C^j_{i(s1)} + \sum_{s2} G_{i(s1),k(s2)} C^j_{k(s2)} \right\} \vec{m}_i \quad (23)$$

The rotational strengths are given by $R_j^T = -\mathrm{Im}\{\vec{\mu}_j^T \cdot \vec{m}_j^T\}$.

To calculate the overall absorption and CD spectra, the homogeneous contributions from excitation to state ϑ_j were expressed as

$$\epsilon_j(\bar{\nu}) = [f^2/n][4\pi^2 N/3000 \ln 10 \hbar c] |\mu_j^T|^2 \bar{\nu}_j \xi_j(\bar{\nu}) \quad (24)$$

and

$$\epsilon_j^{\mathrm{left}}(\bar{\nu}) - \epsilon_j^{\mathrm{right}}(\bar{\nu}) = [f^2/n][16\pi^2 N/3000 \ln 10 \hbar c] R_j^T \xi_j(\bar{\nu}) \quad (25)$$

Here $\bar{\nu}$ is the energy of the measuring light (cm^{-1}); $\bar{\nu}_j$ is the zero-point energy difference between ϑ_j and the ground state; N is Avogadro's number; n is the refractive index of water (1.33); f is the cavity-field correction factor $3n^2/(2n^2+1)$ (see Appendix B), and $\xi_j(\bar{\nu})$ is the line-shape factor:[34]

$$\xi_j(\bar{\nu}) = \sum_{p_1} \cdots \sum_{p_M} B_{\omega,P,T} \sum_{q1} \sum_{q_M} [\prod_{m=1}^{M} \Lambda^{(m)}_{p_m,q_m}] \left[\frac{l^{1/2}\Gamma_j}{2\pi}\right] \Big/ \left\{ \left[\frac{l^{1/2}\Gamma_j}{2\pi}\right]^2 + [\bar{\nu} - \bar{\nu}_j - \hbar \sum_{m=1}^{M} (q_m - p_m)\omega_m]^2 \right\} \quad (26)$$

In eq 26, ω_m is the energy of the mth vibrational mode that couples the ground state to excited state j ($m = 1, 2, ..., M$); p_m and q_m (=0, 1, 2, ..., ∞) are vibrational levels of this mode in the ground and excited states, respectively; $\Lambda^m_{p_m,q_m}$ is the Franck−Condon factor for a vibronic transition between these levels; l (=1, 2, ..., ∞) is the position of (q_1, q_2, ..., q_m) in the ladder of vibrational levels; Γ_j is the homogeneous line width (fwhm) of the $l = 1$ transition; and $B_{\omega,P,T}$ is the Boltzmann weighting factor:

$$B_{\omega,P,T} = \{\exp[-\hbar(\sum_{m=1}^{M} p_m \omega_m)/k_B T]\} / \{\sum_{p_1} \cdots \sum_{p_M} \exp[-\hbar(\sum_{m=1}^{M} p_m \omega_m)/k_B T]\} \quad (27)$$

We included three of the dominant vibrational modes that have been characterized in hole-burning studies on the *Rb. sphaeroides* LH2 complex.[6,35,36] The energies (ω_m) and Huang−Rhys factors (S_m) assigned to these modes are listed in Table 2. Vibrational levels 0−20 were included for each mode up to a cutoff of 3000 cm^{-1}, which provided excellent convergence for the S_m and ω_m values used here. The Franck−Condon factors ($\Lambda^m_{p_m,q_m}$) were evaluated using expressions given by Manneback.[37] A homogeneous line width (Γ_j) of 2.0 cm^{-1} was used for the $l = 1$ transitions of the B800 BChls,[36] 3.75 cm^{-1} for the lowest-energy transition of the B850 BChls,[6,35,36] and (in most of the calculations) 150 cm^{-1} for other $l = 1$ transitions of the B850 BChls including both intramolecular and CT transitions. The assignment of a given transition predominantly to either the B800 or the B850 BChls was made on the basis of the squares of the coefficients ($C^j_{i(s)}$) for the different types of BChl.

Inhomogenous broadening was treated by using a Monte Carlo routine similar to that described by Jimenez et al.[12] to add a Gaussian distribution of uncorrelated perturbations to the diagonal terms of **U**. The zero-point transition energies, dipole strengths, and rotational strengths were stored for 1000 iterations

TABLE 2: Vibrational Parameters

mode	ω^a	$S_{exci}{}^b$	$S_{CT}{}^c$
1	20	0.30	4.0
2	200	0.05	4.0
3	750	0.04	1.0

[a] Energy (cm^{-1}). [b] Huang−Rhys factor (dimensionless displacement) for exciton transitions composed primarily of combinations of local (intramolecular) transitions; from refs 6, 35, and 36. [c] Assumed Huang−Rhys factor for transitions composed primarily of CT transitions. This parameter has not been measured experimentally but is expected to be considerably greater than the S_{exci}.

of the calculations and were averaged over spectral intervals of 10 cm^{-1}. The localization factor $L(\bar{\nu})$ (see below) also was stored for transition energies up to 12700 cm^{-1} on each iteration and then averaged with the same resolution.

Experimental Section

LH2 complexes were prepared from *Rb. acidophila* strain 10050 with lauryldimethylamine oxide as described.[38] Bacteriochlorophyll was assayed spectrophotometrically after extraction into acetone−methanol 7:2 (v:v), using an extinction coefficient of 76 mM^{-1} cm^{-1} at 772 nm.[39] Circular dichroism spectra were measured with the help of Drs. N. Price and S. Kelly at the BBSRC Scottish Circular Dichroism Facility, Stirling, U.K. The low-temperature absorption spectrum was measured with the help of Drs. S. Lin and R. Blankenship at Arizona State University, Tempe, AZ. Molar extinction coefficients were calculated on the assumption that each LH2 complex in the preparation contains 27 molecules of BChl.

Results and Discussion

Measured Absorption and CD Spectra. Figure 2 shows absorption and CD spectra of the *Rp. acidophila* LH2 complex at 293 and 123 K. The spectra measured at 293 K are similar to spectra described previously,[40,41] but give absolute values for the molar extinction coefficients. These values were obtained by measuring the BChl contents of samples with known absorbance (see Methods). For samples suspended in 20 mM Tris HCl, pH 8.0, 0.1% lauryldimethylamine oxide at 293 K, the extinction coefficient at 860 nm was found to be 3.01 ± 0.21 μM^{-1} cm^{-1} (mean and standard error of the mean of eight measurements). Assuming that the 858-nm band is due exclusively to the 18 B850 BChls, the extinction coefficient is equivalent to 0.167 ± 0.012 (μM BChl)$^{-1}$$cm^{-1}$, which agrees well with the value of 0.170 ± 0.005 that Sturgis et al.[42] have measured for B850 in *Rb. sphaeroides*. In 60% glycerol 40% (20 mM Tris HCl, pH 8.0, 0.1% lauryldimethylamine oxide), the solvent used for Figure 2, the B800 and B850 bands both shifted to the red by 0.5 to 1 nm but the widths and peak extinction coefficients were, within experimental uncertainty, the same as in solutions without glycerol. However, the ratio of the two peak extinction coefficients varied over a range of about 10% in samples that were frozen and rethawed. The extinction coefficient quoted by Sturgis et al.[42] for B800 in *Rb. sphaeroides* is about 25% lower than our value in *Rp. acidophila*. As previous workers have described,[6,41] the B850 absorption band shifts to longer wavelengths with decreasing temperature. A notable feature of the CD spectra, which also has been pointed out previously,[7] is that the CD crosses zero significantly to the red of the absorption maxima in both the B800 and the B850 regions. The CD spectrum at low temperatures has not been measured previously to our knowledge.

TABLE 3: Dominant Q_y Exciton Interaction Energies Calculated with Various Treatments of Dielectric Screening

	$U(i,j)$ (cm^{-1})					
i, j^a	$r_o = 2^b$	$r_o = 4$	$r_o = 6$	$r_o = 8$	$r_o = 15$	$r_o = \infty$
$B850^1_\alpha$, $B850^1_\beta$	197	254	436	545	440	394
$B850^1_\alpha$, $B850^2_\beta$	158	209	378	461	345	317
$B800^1$, $B800^2$	−15	−15	−15	15	−15	−30
$B800^1$, $B850^1_\alpha$	−8	−8	−8	−8	−8	17
$B800^1$, $B850^1_\beta$	−2	−2	−2	−2	−2	−4
$B800^1$, $B850^2_\alpha$	16	16	16	16	16	36
$B800^1$, $B850^2_\beta$	4	4	4	4	4	8

[a] BChls. Superscript 1 denotes a BChl in a given $\alpha\beta$ dimer; 2 denotes a BChl in an adjacent dimer. [b] r_o in eq 9 (Å); $n^2 = 2.0$. When $r_o = \infty$, $d_{t1,t2} = 1$, independent of distance; when $r_o = 2$, $d_{t1,t2}$ is effectively fixed at 2.0 because the interatomic distances are all greater than 2 Å.

Calculated Exciton Interaction Energies. Table 3 gives the dominant Q_y exciton interaction energies in the *Rp. acidophila* LH2 complex, as calculated with several treatments of the dielectric screening factor $d_{t1,t2}$ in eq 9. Although the largest interaction energies involve pairs of B850 BChls within $\alpha\beta$ dimers, the interactions of neighboring B850-α and B850-β BChls in adjacent dimers have comparable magnitudes. The interactions involving B800 BChls are weaker by a factor of more than 10. As Sauer et al.[7] have noted, the coupling of each B800 BChl to the second nearest B850 BChl ($B850^2_\alpha$ in Table 3) is about twice as strong as the coupling to the closest B850 ($B800^1_\alpha$).

Dielectric effects are difficult to treat accurately in proteins because of the heterogeneity and anisotropy inherent in protein structures. In principle, a realistic treatment would include the microscopic structure of the protein explicitly in the evaluation of both the diagonal and off-diagonal matrix elements. In the present work we used a simpler and necessarily cruder method of incorporating electrostatic screening in the off-diagonal terms. Because the QCFF/PI orbitals and the CI coefficients are parameterized on the basis of measured optical properties of molecules in solution rather than *in vacuo*, they take into account dielectric screening of the intramolecular electron−electron repulsion integrals. Setting the screening factor $d_{t1,t2}$ in eq 7 equal to 1.0 therefore seems appropriate for short interatomic distances. At large distances $d_{t1,t2}$ should approach the high-frequency dielectric constant (n^2) measured in liquids, which is on the order of 1.8−2.0. For most of the calculations described below, $d_{t1,t2}$ was given the distance dependence specified by eq 9, with $n^2 = 2.0$ and $r_o = 4.0$ Å. Paradoxically, for some values of r_o, the calculated exciton interactions of neighboring B850 BChls are stronger than they would be if $d_{t1,t2}$ were 1.0, independent of distance (see Table 3). This occurs in the particular geometry of the LH2 complex because eq 9 favors contributions from pairs of atoms with shorter interatomic distances; it would not necessarily be true for BChl dimers in other orientations. The effects of varying the choice of r_o on the calculated absorption and CD spectra are discussed in more detail below.

Absorption and Circular Dichroism of a Homogeneous Model. It is instructive to begin calculations of the spectroscopic properties of LH2 with a model in which the monomer transition energies are the same for all BChls of a given structural type, *i.e.* with an interaction matrix **U** that has no diagonal disorder. Absorption and CD spectra calculated for such a model are shown in Figure 3. As in the inhomogeneous models considered below, each LH2 complex has 18 exciton states that result mainly from Q_y excitations of the B850 BChls

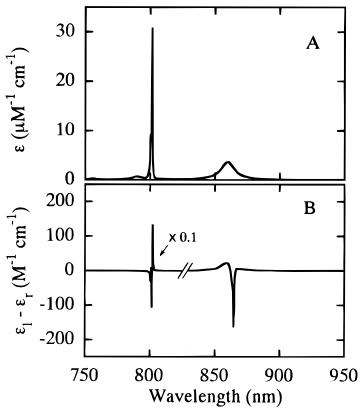

Figure 3. Absorption and (A) and CD (B) spectra calculated for a homogeneous model of the LH2 complex. The monomer transition energies are given in the text and the vibrational parameters in Table 2. Other parameters were $\Gamma_{j>1}^{B850} = 150$ cm^{-1}, $\Gamma_1^{B850} = 3.75$ cm^{-1}, $\Gamma_j^{B800} = 2.0$ cm^{-1}, $n^2 = 2.0$, $r_o = 4$ Å, lowest CT energy = 12 100 cm^{-1}, and $T = 0$ K.

and 9 states that result mainly from Q_y excitations of the B800 BChls. In the first nine of the B850 exciton states, the coefficients (C_i^j) for the Q_y excitations of a given B850-α-B850-β dimer generally have opposite signs (Figure 4). The 0−0 excitation energies of these 9 states are calculated to fall in the range of 11 600−12 200 cm^{-1} (820−862 nm). In states 10−18, the corresponding coefficients generally have the same sign, and the excitation energies are in the region of 12 400−12 650 cm^{-1} (790−806 nm). The lowest 9 B850 states thus are constructed, to a first approximation, of antisymmetric exciton states of B850 αβ dimers, and the upper nine of symmetric dimer states. However, several factors make this description only approximate even within the confines of the homogeneous model. First, the magnitudes of C_i^j for the two Q_y excitations in an αβ B850 dimer are different because the β BChls have lower intramolecular Q_y transition energies. Second, the intramolecular Q_y transitions are mixed to various extents with CT transitions. And third, as noted above, excitonic coupling of B850 BChls in adjacent dimers is almost as strong as the coupling within a dimer (Table 3).

In the B850 state with the lowest energy, the squares of the coefficients for the local Q_y excitations ($|C_{i(s)}^j|^2$) are 0.050 for all the B850 α BChls and 0.056 for the β BChls (see Figure 4A). The probability of finding a Q_y excitation on a particular molecule in this state thus is nearly constant around the B850 ring. The $|C_{i(s)}^j|^2$ for the 18 B850 Q_y excitations sum to 0.954, indicating that about 5% of the excitations represent higher-energy local transitions, CT transitions, and transitions of the B800 BChls. Because the vector sum of the Q_y transition dipoles of the individual B850 molecules is close to zero, the dipole strength associated with the lowest-energy state is extremely small and makes no significant contribution to the absorption spectrum. This result can be derived easily from a group theoretical representation. In the homogeneous model, the circular array of BChls in the *Rp. acidophila* LH2 complex has C_9 symmetry. The lowest- and highest-energy exciton levels of the ring are described by the *A* irreducible representation of the C_9 point group, in which only transitions normal to the ring plane are allowed. Because the individual transition dipoles of the B850 BChls lie nearly in this plane, the dipole strength for excitations into either of the *A* states is very small. The B850 absorption band arises almost exclusively from excitations into a degenerate pair of exciton states with E_1 character, which lie approximately 60 cm^{-1} above the forbidden *A* state and have orthogonal transition dipoles in the plane of the ring (Figure

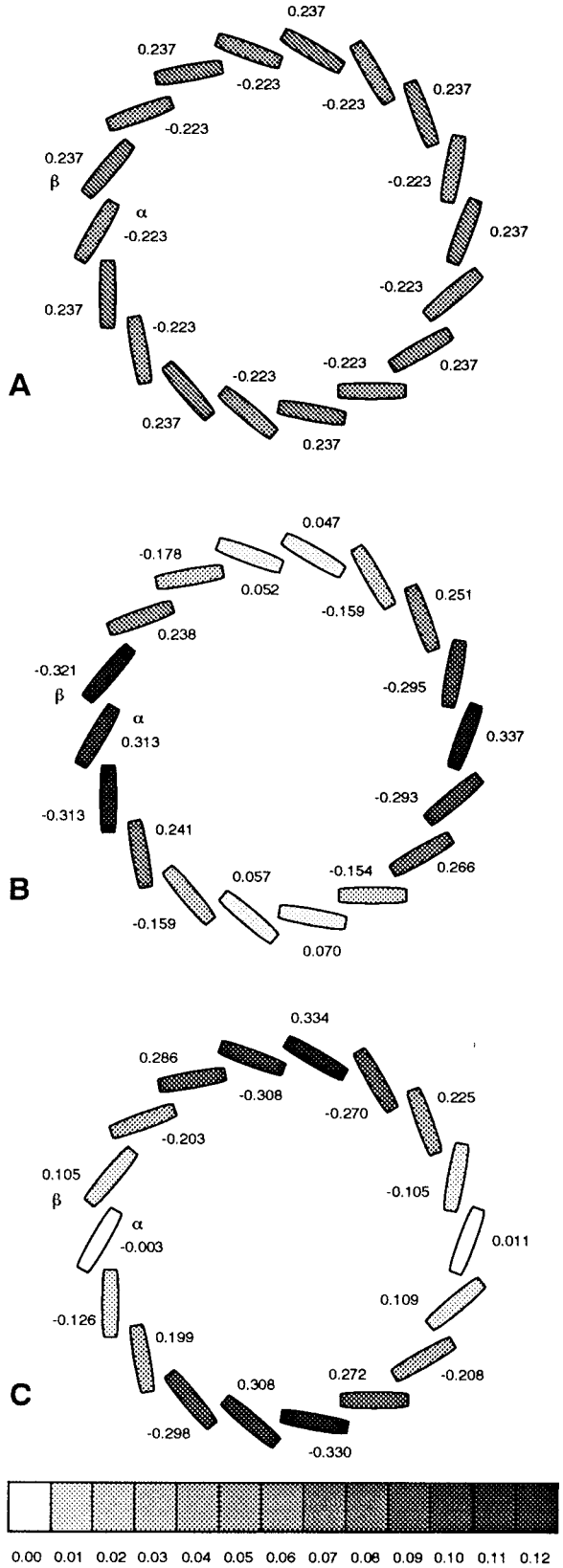

Figure 4. Coefficients of the B850 Q_y transitions in lowest three eigenstates of a homogeneous model of the LH2 complex. Panel A is the lowest excited state; B and C are the two degenerate states just above the lowest. Coefficients for α BChls are indicated inside the rings, coefficients for β BChls, outside. The gray scale (bottom) indicates the squares of the coefficients.

4B,C). The other excited states of the B850 array can be described by E_2, E_3, and E_4 irreducible representations, and all are formally dipole-forbidden. These general features of circular

antenna systems have been pointed out previously by several investigators.[6,7,12,43−46]

If we consider either one of the two allowed exciton states alone, the $Q_y |\mathbf{C}^j_{i(s)}|^2$ vary from molecule to molecule (see Figure 4B,C). However, the sums of the $|C^j_{i(s)}|^2$ for the two E_1 states are the same for all molecules of a given type (0.098 for α BChls and 0.114 for β). Because there is no way to prepare a pure system in one of these degenerate states, the measurable excitation density would be nearly constant around the ring.

Although the antisymmetric *A* excitation carries little dipole strength, it has a large magnetic transition dipole normal to the plane and a negative rotational strength on the order of −10 D·μ_B (debye·Bohr magneton). The two dipole-allowed E_1 states both have in-plane magnetic transition dipoles and positive rotational strengths on the order of 8 D·μ_B. The homogeneous model thus accounts qualitatively for the positive and negative CD bands seen in the 860-nm region (Figure 2B).

The nine exciton states that arise predominantly from Q_y transitions of the B800 BChls are clustered near 12 500 cm^{-1} (800 nm). This puts the B800 exciton states close to resonance with some of the upper exciton components of the B850 ring. Because the monomeric B800 transitions are degenerate in the homogeneous model, the exciton states obtained by diagonalizing **U** are inherently delocalized over the entire complex. They can be described by the same *A*, E_1, E_2, E_3, and E_4 irreducible representations used for the B850 states, and again only the two degenerate E_1 excitations are allowed. However, this treatment is not physically realistic because variations in the local environments of the BChls give the monomer transitions a distribution of energies. If the difference between the Q_y energies of neighboring molecules is larger than the interaction matrix elements, the B800 transitions will tend to localize on individual molecules or small sets of molecules. We turn now to a model that incorporates this effect for both the B800 and the B850 BChls.

Effects of Inhomogeneity. The forbidden transitions of the B800 and B850 BChls can gain dipole strength as a result of inhomogeneities that perturb the symmetry of the chromophore rings. Such inhomogeneity must exist at some level in any biological system, given the glasslike nature of proteins.[47] To explore how inhomogeneity disrupts the exciton structure of the LH2 complex, we used a Monte Carlo routine to give the $\pi \rightarrow \pi^*$ and CT basis transitions uncorrelated Gaussian distributions of transition energies. Absorption and CD spectra were averaged over 10^3 iterations of the calculations. Figure 5 shows absorption spectra obtained with four values of the standard deviation of the energy distribution for the basis transitions involving the B850 BChls (σ_{B850} = 100, 130, 200, and 300 cm^{-1}). The transitions of the B800 BChls were given a standard deviation (σ_{B800}) of 130 cm^{-1} in all four cases, in accord with the results of hole-burning studies on B800 in *Rb. sphaeroides* and *Rp. acidophila*.[35,36,48] As in the homogeneous model, the calculations give strong absorption bands in the regions of 800 and 860 nm. However, transitions into the lowest-energy exciton state now appear as a shoulder on the red side of the B850 band, which becomes increasingly prominent as σ for the B850 BChls is increased. Such a shoulder has been seen in spectra measured experimentally at 4 K,[6] although it is not resolved in the spectra shown in Figure 2. Wu et al.[6] place the peak of the low-energy band 200 cm^{-1} below the main absorption peak and estimate the area under the band to be approximately 3% of the total area of the B850 absorption band.

Hole-burning action spectra have shown that the low-energy feature of the B850 band has a width (fwhm) in the range of 60 cm^{-1} to 120 cm^{-1} in *Rp. acidophila* (depending on the sample) and approximately 100 cm^{-1} in *Rb. sphaeroides*.[6,35,36] The zero-phonon hole for this transition has a width of about 3.2 cm^{-1}, which corresponds to a homogeneous lifetime (T_2) of ∼7 ps. The total width of 60−120 cm^{-1} presumably reflects site inhomogeneity in the monomer transition energies, the interaction matrix elements, or both. Figure 5 shows that as the inhomogeneity of the monomer energies is increased the low-energy band broadens and moves to longer wavelengths relative to the absorption maximum. The calculated intensities, widths, and positions of the low-energy band are given in Table 4. The spectral properties calculated with $\sigma_{B850} \approx$ 100−130 cm^{-1} are in reasonably good accord with the properties measured experimentally,[6] although the relative strength of the low-energy shoulder is somewhat too large and the energy separation from the main absorption maximum is smaller than observed. Setting σ_{B800} and σ_{B850} in the range of 130 cm^{-1} also gives good agreement with the overall absorption spectrum. The 800-nm band is broader than observed, but this could reflect the simplifications in our treatment of the homogeneous line widths of the upper B850 transitions (see below).

For the model with σ_{B850} = 130 cm^{-1}, the calculated energy separation between the absorption maxima of the low-energy band and the main B850 band is 79 cm^{-1} (Table 4). This separation is larger than the mean energy gap between the lowest state and the higher, allowed states because the absorption in the low-energy band is weighted strongly in favor of trials that yield larger values of the energy gap. Figure 6 illustrates the relationship between the dipole strength of the lowest excitation and the energy gap separating the lowest state from the next two states above it. Whereas the distribution of the energy gap

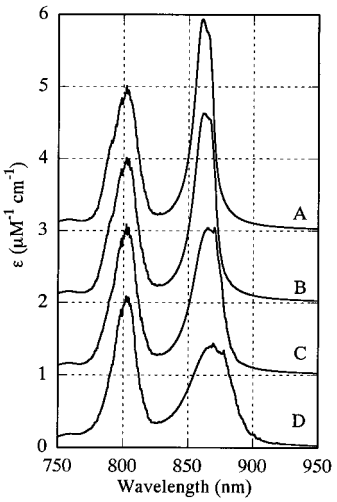

Figure 5. Absorption spectra calculated using uncorrelated Gaussian distributions of the basis transition energies, with σ_{B800} = 130 cm^{-1} and σ_{B850} = 100 (A), 130 (B), 200 (C), or 300 (D) cm^{-1}. Other parameters were as in Figure 3. The ordinate scale is for spectrum *D*; the other spectra are displaced vertically in increments of 1 μM^{-1} cm^{-1}.

TABLE 4: Calculated Properties of the Low-Energy Band[a]

σ_{B850} (cm^{-1})	peak[b,c] (cm^{-1})	relative area[d] (%)	width[c,e] (cm^{-1})
100	−67	6	70
130	−79	8	90
200	−79	12	130
300	−110	12	210

[a] Each line represents the mean of 1000 iterations of the calculations with the indicated value of σ_{B850} and other parameters as in Figure 5. [b] Peak position (Franck−Condon maximum) relative to the main absorption maximum. [c] Calculated for T = 0 K with the vibrational parameters of Table 2, $\Gamma^{B850}_{j>1}$ = 150 cm^{-1}, and Γ^{B850}_1 = 3.75 cm^{-1}. [d] Area relative to the main absorption band. [e] fwhm.

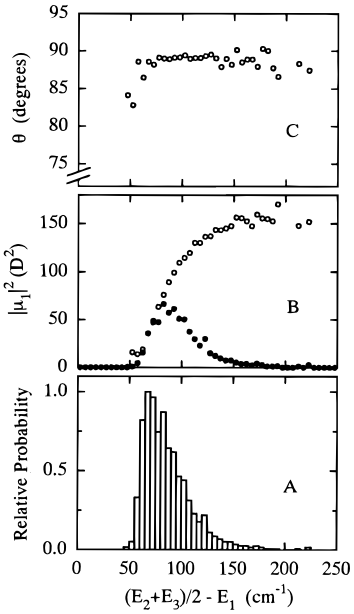

Figure 6. Properties of the lowest exciton transition, calculated by 1000 Monte Carlo variations of the basis transition energies with $\sigma_{B850} = 130$ cm^{-1} and other parameters as in Figure 3. The abscissa [$(E_2 + E_3)/2 - E_1$] is the difference between the energy of the lowest transition and the mean energy of the next two transitions. Calculated properties were averaged over energy intervals of 5 cm^{-1}. (A) Normalized distribution of $(E_2 + E_3)/2 - E_1$. (B) Dipole strength of the lowest transition (○) and the product of the dipole strength and the relative probability of having the indicated energy difference (●). (C) Angle (θ) between the C_9 symmetry axis and the transition dipole of the lowest exciton transition.

$[(E_2 + E_3)/2 - E_1]$ peaks in the range of 65−70 cm^{-1} (Figure 6A), configurations of diagonal energies that give larger energy differences transfer more dipole strength to the lowest excitation and thus contribute disproportionately to the shoulder of the absorption spectrum (Figure 6B). This point could have significant consequences for the interpretation of time-resolved spectral data at low temperatures because energy transfer among an inhomogeneous ensemble of LH2 complexes would result in a red shift of the fluorescence.

Figure 6C shows how the calculated angle (θ) between the C_9 symmetry axis and the transition dipole of the low-energy transition depends on $(E_2 + E_3)/2 - E_1$. As was mentioned above, θ would be zero for a homogeneous system with C_9 symmetry. However, because the transition dipoles of the individual B850 BChls are nearly perpendicular to the symmetry axis, relatively small amounts of inhomogeneity are sufficient to tip θ to values in the region of 90°. The dominant transition dipoles in the low-energy band thus would be nearly coplanar with the transition dipoles associated with the main B850 absorption band, but on average would have no preferred orientation in this plane. This agrees with the experimental observation that the fluorescence of oriented LH2 complexes is polarized in the plane of the ring[49] and with the fluorescence anisotropy of approximately +0.1 measured when the LH2 complex is excited in the B850 band.[8,50] By contrast, a fluorescence anisotropy of −0.2 would be expected for the weak emission from the *A* state of a homogeneous system.

Figure 7 shows the calculated CD spectra obtained with $\sigma_{B850} = 100$, 130, 200 and 300 cm^{-1}. Again, the results obtained with σ_{B850} in the range of 100−130 cm^{-1} agree well with the experimental spectrum (Figure 2B). As in the homogeneous model, a major band with negative rotational strength is found on the red side of the B850 region and a positive band on the blue side. Because the negative CD band is associated with

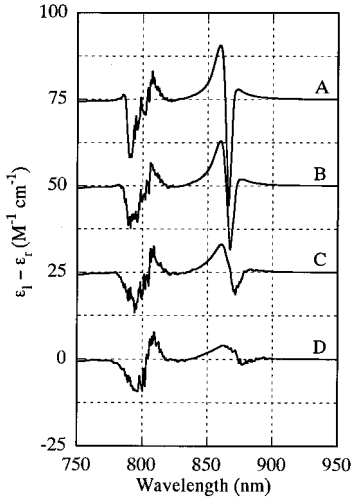

Figure 7. CD spectra calculated as in Figure 5 with $\sigma_{B800} = 130$ cm^{-1} and $\sigma_{B850} = 100$ (A), 130 (B), 200 (C), or 300 (D) cm^{-1}. The ordinate scale is for *D*; the other spectra are displaced vertically in increments of 25 M^{-1}cm^{-1}.

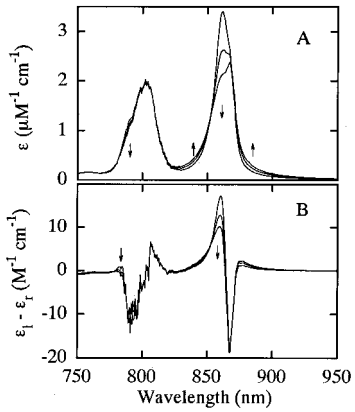

Figure 8. Absorption (A) and CD (B) spectra calculated as in Figures 5 and 7, but with σ_{B850} fixed at 130 cm^{-1} and $\Gamma_{j>1}^{B850} = 100$, 150, or 200 cm^{-1}. Arrows indicate the direction of increasing $\Gamma_{j>1}^{B850}$.

the shoulder on the absorption band, the calculated CD crosses zero to the red of the absorption maximum, in accord with experiment. Sauer et al.[7] have noted that this displacement is difficult to explain on the assumption that excitations are restricted to small groups of pigments but arises naturally in models that include delocalized exciton states. The pair of positive and negative bands in the 800-nm region is due primarily to transitions of the B800 BChls, with higher-energy B850 states contributing a broad negative band near 790 nm and a broad positive band at shorter wavelengths.

Homogeneous Line Widths. The detailed shapes of the calculated absorption and CD spectra depend on the homogeneous line widths (Γ) assigned to the transitions (see eqs 26 and 27). The spectra presented in Figures 5 and 7 were generated by using a homogeneous line width ($\Gamma_{j>1}^{B850}$) of 150 cm^{-1} for all the B850 Q_y exciton levels other than the lowest. Figure 8 shows the dependence of the calculated spectra on the choice of this width. The homogeneous line widths for the lowest B850 exciton level (Γ_1^{B850}) and for all the B800 levels (Γ_j^{B800}) were fixed at 3.75 and 2.0 cm^{-1}, respectively, in accord with the widths of zero-phonon holes burned on the red sides of the 850- and 800-nm absorption bands at low temperatures.[6,35,36] Setting $\Gamma_{j>1}^{B850}$ at 150 cm^{-1} gives the 850-nm band approximately the correct overall width and also matches the relative peak heights of the B850 and B800 bands when σ_{B850} and σ_{B800} are 130 cm^{-1}. The negative CD band at long

wavelengths is much less sensitive to $\Gamma_{j>1}^{B850}$ than the positive band just above it, again because it is associated mainly with the lowest exciton level.

For a discrete excited state, a homogeneous line width of 150 cm^{-1} would correspond to a lifetime (T_2) of ~35 fs. In pump−probe studies of *Rb. sphaeroides* chromatophores at room temperature, Nagarajan et al.[51] recently measured time constants of approximately 20 and 35 fs for the decay of anisotropy and a relaxation of the stimulated emission and excited-state absorption of B850. These time constants were interpreted as reflecting electronic dephasing and relaxation from strongly-allowed exciton states into a weakly-allowed state at lower energies. In hole-burning studies of *Rb. sphaeroides* and *Rp. acidophila* LH2 complexes at 4 K, Small and co-workers[6,35,36] have measured sample-dependent, aggregate homogeneous line widths on the order of 200 cm^{-1}. However, these measurements give the envelope (or exciton bandwidth) of the zero-phonon holes of all exciton levels with significant dipole strength in the 850-nm region. The measured hole width is, therefore, necessarily broader than the homogeneous width associated with a single level. A homogeneous line width of 150 cm^{-1} for the individual B850 transitions thus seems reasonable, although the use of a single value of Γ for all of these transitions is clearly an approximation. The line widths of the high-lying exciton states are likely to be broader than those of lower levels due to the existence of multiple decay pathways from the higher states. Zero-phonon hole widths measured on the blue side of the 800-nm absorption band, for example, are larger than those measured on the red side.[48]

The calculated spectra in Figures 5 and 8 include a shoulder on the blue side of the 800-nm band, which reflects absorption into the upper exciton states of the B850 chromophores. Reddy et al.[36] have observed that hole-burning into the B850 band produces a broad satellite hole at ~785 nm and have assigned this feature to a vibronic band centered approximately 920 cm^{-1} above the B850 absorption maximum. Their assignment was based largely on a peak seen in high-resolution fluorescence excitation spectra of monomeric BChl-*a* at low temperature.[52] Our calculations favor assigning the 785-nm feature to upper exciton components of B850 but do not provide a basis for predicting the homogeneous line width of these states. As pointed out above, the B850 exciton transitions in the 780 nm region could have large homogeneous widths due to rapid relaxation into lower exciton levels of B850 and/or B800. Using a larger homogeneous line width for the upper B850 transitions would disperse their contributions to the absorption spectrum and sharpen the remaining 800-nm band of the B800 BChls.

Effects of CT Transitions. For the calculations described thus far, the energy of the lowest CT transition between adjacent B850 $\alpha\beta$ dimers ($\alpha\phi_2 \rightarrow \beta\phi_3$) was fixed at 12 100 cm^{-1}, which is in the range of the CT energies suggested for *Rp. viridis* reaction centers.[16] The energies of the higher CT transitions were positioned above this by the relative values of $\Delta E^{gas} + \Delta V^{QQ}$ given in Table 1. Similar results (not shown) were obtained if the relative CT energies were set by ΔE^{gas} alone. Because the model did not include the protein explicitly, the CT energies could not be calculated independently. If all of the CT states were raised by 10 000 cm^{-1} to move them far out of resonance with the B850 Q_y transitions, the calculated B850 absorption band maximum shifted to the blue by 121 cm^{-1}, the mean dipole strength of the lowest exciton band increased from 75.5 to 87.4 D^2, and the mean rotational strength of this band decreased in magnitude from −5.7 to −5.1 $D{\cdot}\mu_B$. However, CT states appear to be much less important in the LH2 complex than they are in reaction centers,[16] where the distance between the macrocyclic planes of the special pair of BChls is shorter by about 0.4 Å. As discussed in Methods, mixing of CT transitions with local excitations falls off abruptly with distance.

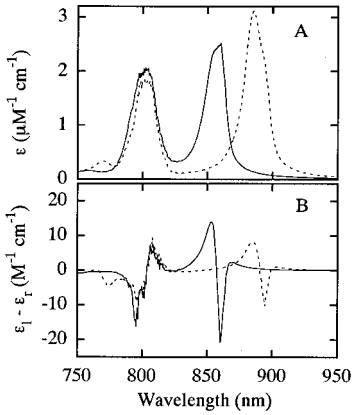

Figure 9. Absorption (A) and CD (B) spectra calculated as in Figures 5 and 7, but with σ_{B850} fixed at 130 cm^{-1} and r_o = 2 (—) or 6 (···) Å.

The conclusion that CT transitions make, at most, only small contributions to the spectroscopic properties is consistent with the observation that electron−phonon coupling is considerably weaker in the LH2 complex than it is in reaction centers.[35,36] Strong electron−phonon coupling (a Huang−Rhys factor greater than 1.0) is expected for systems where the excitation causes a significant change in dipole moment and, consequently, a large change in equilibrium nuclear positions.[53] The Huang−Rhys factors of considerably less than 1.0 that have been measured for the 800- and 850-nm absorption bands of the LH2 complex (see Table 2) are comparable to those of monomeric BChl-*a* in solution.[52] The Stokes shift, which provides another measure of nuclear displacements in the excited state, also is smaller in the LH2 complex than in reaction centers; the Stokes shift for the *Rb. sphaeroides* LH2 complex at 295 K is 84 cm^{-1},[9] compared to approximately 535 cm^{-1} for *Rb. sphaeroides* reaction centers.[54]

Exciton states with little CT character often display narrowed absorption spectra relative to the monomeric species.[55,56] The measured widths (fwhm) of the B800 and B850 bands of the LH2 complex at 293 K are approximately 320 and 415 cm^{-1}, respectively (Figure 2). Widths reported for monomeric BChl in solution range from 515 cm^{-1} in CCl_4 to 930 cm^{-1} in methanol.[57] The absorption bands thus are narrowed modestly in the LH2 complex, although this could be attributable to the more ordered environment of the pigments in the protein. As discussed above, rapid relaxations among the exciton states probably broaden the B850 band homogeneously relative to B800.

Effects of Dielectric Screening. For the calculations described above, effects of dielectric screening were treated by using eqs 7 and 9 with r_o = 4 Å. We carried out similar calculations with r_o = 2, 6 and 8 Å, and also with $d_{t1,f2}$ fixed at 1 ($r_o = \infty$). Figure 9 shows representative absorption and CD spectra obtained with r_o = 2 and 6 Å. As r_o is increased over this range, the B850 band shifts to longer wavelengths and grows in strength while the positive and negative CD bands at long wavelengths become weaker. The 800-nm band sharpens as the higher-energy exciton states of the B850 BChls move out of resonance with the B800 states. However, the qualitative features of the absorption and CD spectra are largely preserved. A value of r_o in the region of 4 Å seems physically realistic because it corresponds roughly to the limit of parameterizations based on intramolecular properties. (See Note Added in Proof.)

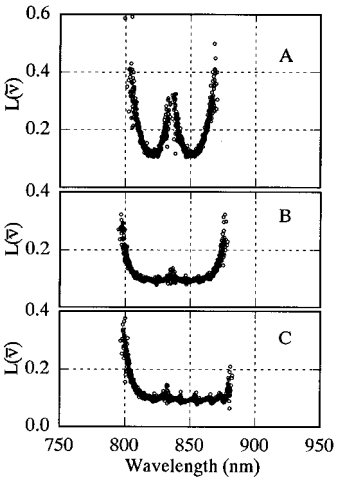

Figure 10. Localization function, averaged over energy intervals of 10 cm^{-1}, for a model that considers only the Q_y transitions of the B850 BChls. The monomer transition energies had a mean of 11 968 cm^{-1} and a standard deviation of 85 cm^{-1}; 10^3 Monte Carlo variations of the energies were made. (A) With only nearest-neighbor interactions and the exciton-interaction matrix elements given by Jimenez et al.[12] (B) With only nearest-neighbor interactions; matrix elements calculated by eqs 8−11 with $n^2 = 2.0$ and $r_o = 4$Å. (C) Including Q_y exciton interactions of all 18 B850 BChls; matrix elements as in part B.

Localization of the Exciton States. As was mentioned above, inhomogeneity in the LH2 complex could cause the exciton states to be localized on small groups of BChls. Fidder et al.[58] have considered such localization in linear aggregates with diagonal and off-diagonal disorder. They define the degree of localization for states at energy $\bar{\nu}$ as:

$$L(\bar{\nu}) = \langle \sum_i (C_i^j)^4 \rangle_{\bar{\nu}} \qquad (28)$$

As above, C_i^j is the coefficient of basis state i in excited state j of the complex; $\langle ... \rangle_{\bar{\nu}}$ represents an average over all states j with energies in a small interval $\bar{\nu} \pm \delta/2$. An excited state due to a single transition of an individual molecule has $L(\bar{\nu}) = 1.0$, while a state representing a uniform distribution of a single type of transition over N molecules would have $L(\bar{\nu}) = 1/N$. A smaller value of $L(\bar{\nu})$ thus implies a more delocalized state. The value of $L(\bar{\nu})$ at the 0−0 transition energy cannot, however, be interpreted simply as the reciprocal of the number of molecules that participate in an excited state. The two allowed exciton states of the homogeneous model are properties of the entire B850 ring and yet give $L(\bar{\nu}) \approx 0.076$ rather than 0.056 ($^1/_{18}$) because the $|C_i^j|$ are not the same for all 18 BChls in each individual state (see Figure 4B,C). Conversely, mixing with higher-energy local excitations and CT transitions will decrease $L(\bar{\nu})$ even if the coefficients for this mixing are the same for all the molecules. For the forbidden, low-energy state of the homogeneous model, which includes about 5% excitations other than B850 Q_y transitions (see above), $L(\bar{\nu})$ is 0.051.

Jimenez et al.[12] have used a Monte Carlo method to calculate $L(\bar{\nu})$ for a model that considered only the Q_y transitions of the B850 BChls and only nearest-neighbor interaction matrix elements. The B850α and β BChls were assumed to have the same mean 0−0 transition energy (11 968 cm^{-1}). We have reproduced their results by using the same interaction matrix elements and mean 0−0 transition energies. The $L(\bar{\nu})$ values plotted in Figure 10A show the results from 10^3 calculations with $\sigma_{B850} = 85$ cm^{-1} (fwhm = 200 cm^{-1}). As Jimenez et al. found, $L(\bar{\nu})$ is approximately 0.14 at the 858-nm absorption maximum and rises steeply at longer wavelengths. Figure 10B shows similar calculations that again consider only Q_y transitions and only nearest-neighbor interactions, but with the interaction matrix elements calculated in the present paper (254 and 209 cm^{-1} for intra- and interdimer interactions, respectively, as compared to the values of 230 and 110 cm^{-1} used by Jimenez et al.). Using the larger matrix elements shifts the absorption maximum to 868 nm and decreases $L(\bar{\nu})$ at this wavelength to 0.12. Figure 10C shows calculations of $L(\bar{\nu})$ that still retain the mean Q_y 0−0 transition energy used by Jimenez et al. but include the off-diagonal matrix elements involving Q_y transitions of non-nearest neighbors in the B850 ring. The inclusion of the additional off-diagonal matrix elements shifts the absorption maximum to 870 nm and reduces $L(\bar{\nu})$ here to 0.09. These results point to the importance of including all the significant interaction terms in the calculations and of using as realistic a model as possible to evaluate the off-diagonal matrix elements.

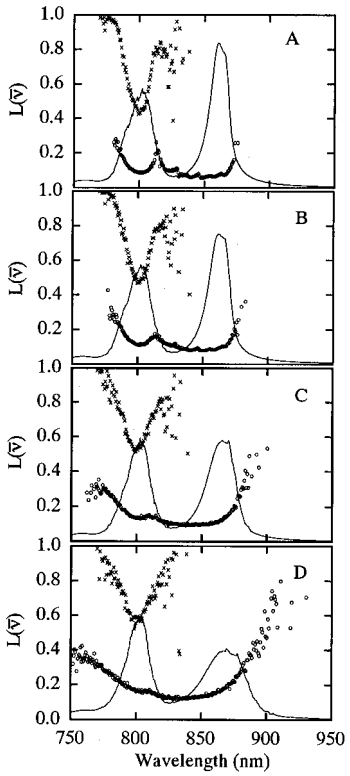

Figure 11. Localization functions for B850 (○) and B800 (×) states, averaged over energy intervals of 10 cm^{-1}, calculated using the full interaction matrix as in Figure 5 with $\sigma_{B800} = 130$ cm^{-1} and $\sigma_{B850} =$ 100 (A), 130 (B), 200 (C), or 300 (D) cm^{-1}. The calculated absorption spectra also are shown.

Figure 11 shows the values of $L(\bar{\nu})$ obtained with the full interaction matrix, including CT states and the Q_y, Q_x, B_x, and B_y transitions of all 27 BChls, and with our values for the mean 0−0 monomer transition energies (12 500 cm^{-1} for B800, 12 284 cm^{-1} for B850-β, and 12 193 cm^{-1} for B850-α BChls). The $L(\bar{\nu})$ terms were calculated separately for states of predominantly B800 $\pi\pi^*$ character and B850 $\pi\pi^*$ character. States with more than 50% CT character were not included in the computations of $L(\bar{\nu})$. (No states with dominant CT character were found below 12 100 cm^{-1}.) As in Figure 5, calculations were done with four values of σ_{B850} (100, 130, 200, and 300 cm^{-1}); a standard deviation of 130 cm^{-1} was used for the B800 transitions in all cases. With values of σ_{B850} that are consistent with the observed absorption and CD spectra (100−130 cm^{-1}), $L(\bar{\nu})$ remains below 0.1 over most of the B850 absorption band, indicating that excitations are extensively delocalized over the B850 ring. The higher value of $L(\bar{\nu})$ in the B800 absorption

band (0.6) indicates that excitations here are considerably more localized, although they still appear to spread over more than one BChl.

Concluding Remarks

Although the details of the spectra depend to some extent on the treatment of dielectric screening, on the energies assigned to the monomeric pigments, and on adjustable parameters such as the CT energies and homogeneous line widths, the calculated absorption and CD spectra are in good accord with experiment and the qualitative results are reasonably robust to alterations in the theoretical parameterization. Experimental results from hole-burning studies have been incorporated wherever possible in the treatment of the homogeneous and inhomogeneous line widths and the frequencies and Huang−Rhys factors of the dominant vibrational modes. This experimental information aids particularly in determining the contributions of inhomogeneity to the spectra. More accurate transition energies for the monomers might be obtained by considering hydrogen bonding and other interactions with the protein explicitly and possibly by using INDO calculations[59,60] in place of QCFF/PI. Sturgis et al.[61,62] have suggested that the shift of the monomeric BChl absorption from 780 nm to the region of 800 nm in the LH2 complex results mainly from hydrogen bonding to the 2-acetyl group.

It is important to note that the crystal structure of the LH2 complex was determined at room temperature and that the calculated interaction matrix elements were based on this structure, whereas the hole-burning studies[6,35,36,48] that provided estimates of the vibronic parameters and the homogeneous line widths Γ_j^{B800} and Γ_1^{B850} were carried out at 4 K. The value of 150 cm^{-1} used for $\Gamma_{j>1}^{B850}$ was based partly on the hole-burning results, but also on time-resolved measurements at room temperature.[51] For simplicity, all the spectral line shapes were calculated for 0 K. The spectra are expected to broaden at higher temperatures, but probably not exactly as predicted by eqs 26 and 27 with fixed values of Γ_j^{B800}, Γ_1^{B850} and $\Gamma_{j>1}^{B850}$. As Wu et al.[6] have noted, the shift of the B850 absorption band to the red (Figure 2) suggests that interactions among the BChls are stronger at low temperatures than at room temperature.

The results presented here indicate that, at early times after the absorption of light, excitations of the B850 BChls in *Rp. acidophila* are delocalized extensively over the ring of 18 pigments. This contrasts with the conclusions of several investigators,[12,43,63−66] who have suggested that excitations are localized on groups of 2−5 BChls. However, recent measurements of the magnitude[67] and anisotropy[51] of flash-induced absorbance changes appear to support the view that the exciton states of LH2 complexes in *Rb. sphaeroides* and *Chromatium tepidum* are strongly delocalized. Measurements of the magnitudes of flash-induced absorbance changes suggest that the exciton states of LH1 antenna complexes also involve a large fraction of the BChls,[45,67−69] although other workers[46,65,70,71] again have favored more localized excitations. In the present calculations, increased localization is seen in the B800 band and on the red edge of the B850 band where the absorption is weighted in favor of complexes with atypically large diagonal disorder (Figures 6 and 11), but the calculated values of $L(\bar{\nu})$ suggest that even excitations in the B800 band are initially delocalized to a significant extent.

Although the calculated spectral line shapes include homogeneous broadening, we have not explicitly considered relaxations that could cause excitations to become increasingly localized with time.[72] One observation that may be difficult to reconcile with the persistence of strongly delocalized excitations is that the fluorescence quantum yield from the LH2 complex increases with decreasing temperature.[41,73,74] Unless the fluorescence lifetime also increases substantially, the fluorescence yield should decline as k_BT drops below the $E_2 - E_1$ energy gap of approximately 60 cm^{-1}. Between 300 and 77 K, the increase in fluorescence yield appears to be explained by a corresponding increase in the fluorescence lifetime,[72] which presumably reflects a slowing of nonradiative decay processes. However, the fluorescence lifetime seems not to have been measured at temperatures below 77 K, where the yield continues to increase.[41,73]

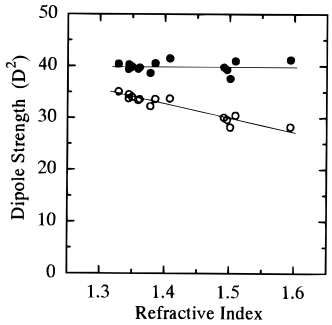

Figure 12. Dipole strength of monomeric BChl-*a* in 14 solvents as a function of the refractive index, calculated from experimental data of Connolly et al.[61] with two different treatments of the local-field correction factor (*f*). ○, $f = (n^2 + 2)/3$; ●, $f = 3n^2/(2n^2 + 1)$.

In work to be presented elsewhere, we have used the model described here to calculate changes in the absorption and emission spectra that would be caused by excitation of the LH2 complex and also to calculate Stark effects on the absorption spectrum. Comparisons with the measured Stark spectrum[75] allow more accurate positioning of the CT energies than is possible by modeling only the absorption and CD spectra.

Note Added in Proof: Equation 9 does not include the local-field correction factor *f* explicitly. Including such a correction would reduce the effective value of n^2, resulting in a small increase in the B850 Q_y exciton-interaction matrix elements for $r_o = 2$ or 4 Å and a decrease for $r_o = 6$, 8, or 15 Å.

Acknowledgment. We thank Nicholas Price and Sharon Kelly (BBSRC Scottish Circular Dichroism Facility) for help with the CD measurements, Su Lin and Robert Blankenship (Arizona State University) for measuring the low-temperature absorption spectrum, and Gerald Small (Iowa State University), Kenneth Sauer (University of California, Berkeley), and Neil Isaacs, Andy Freer, and Stephen Prince (University of Glasgow) for much helpful discussion. The work at the University of Washington was supported by NSF Grant MCB-95-13229 and that at the University of Glasgow by the BBSRC. C.J.L. was supported by a BBSRC postgraduate fellowship and E.J.J., in part, by an NIH predoctoral training grant in molecular biophysics (5-T32-GM08268-09).

Appendix A. Matrix Elements of $\tilde{\nabla}$

The Slater $2p_z$ orbital, in polar coordinates centered on the atom, can be written $\chi = (\zeta^5/\pi)^{1/2}\, r \cos\theta \exp\{-\zeta r\}$ with $\zeta =$ 3.685, 4.299, and 3.071 $Å^{-1}$ for N, O, and C, respectively. The matrix elements $\langle\chi_2|\tilde{\nabla}|\chi_1\rangle$ are functions of the interatomic distance (*R*) and the ζ parameters for the two atoms (ζ_1 and ζ_2). Let $p = (\zeta_1 + \zeta_2)R/2$, $q = (\zeta_2 - \zeta_1)R/2$, $A_k = \int_1^\infty w^k \exp(-pw)\, dw$ and $B_k = \int_{-1}^1 w^k \exp(-qw)\, dw$. Then, following procedures described by Mulliken et al.,[76] Král,[77] and Harada and Nakanishi,[78] we find

$$\nabla_\sigma = (\zeta_1\zeta_2)^{5/2}(R^4/8)\{A_0B_2 - A_2B_0 + A_1B_3 - A_3B_1 + (\zeta_1 R/2)[A_1(B_0 - B_2) + B_1(A_0 - A_2) + B_3(A_4 - A_2) + A_3(B_4 - B_2)]\} \quad \text{(A1)}$$

$$\nabla_\pi = (\zeta_1\zeta_2)^{5/2}(\zeta_1 R^5/32)\{(B_1 - B_3)(A_0 - 2A_2 + A_4) + (A_1 - A_3)(B_0 - 2B_2 + B_4)\} \quad \text{(A2)}$$

$$\nabla_{xy} = (\zeta_1\zeta_2)^{5/2}(R^4/8)\{A_0B_2 - A_2B_0 + A_1B_3 - A_3B_1 + (\zeta_1 R/4)[(A_3 - A_1)(B_0 - B_4) + (B_3 - B_1)(A_0 - A_4)]\} \quad \text{(A3)}$$

Equations A2 and A3 were given previously by Král.[77] A_k and B_k can be evaluated with expressions given by Miller et al.:[79]

$$A_k = (e^{-p} + kA_{k-1})/p \quad \text{(A4)}$$

$$B_k = 2\sum_{i=0}^{3}[q^{2i}/(2i)!(k + 2i + 1)] \qquad \text{for } k \text{ even} \quad \text{(A5)}$$

$$B_k = -2\sum_{i=0}^{3}[q^{2i+1}/(2i + 1)!(k + 2i + 2)] \qquad \text{for } k \text{ odd} \quad \text{(A6)}$$

Appendix B. The Dipole Strength of BChl-*a*

There is some uncertainty in the choice of the experimental dipole strengths because the absorption spectrum of BChl-*a* depends on the solvent. The dipole strength is related to the molar extinction coefficient (ϵ) by the expression

$$|\vec{\mu}|^2 = (3000 \ln 10\hbar c/8\pi^3 N)(n/f^2)\int(\epsilon/\nu)\mathrm{d}\nu \quad \text{(B1)}$$

where N is Avogadro's number, n is the refractive index of the solvent, f is the local-field correction factor, and ν is the frequency. Connolly et al.[57] have reported on the absorption maximum ($\bar{\nu}_o$), peak molar extinction coefficient (ϵ_o), and full width at half-height (W) of the Q_y absorption band of BChl-*a* in 14 solvents covering a wide range of polarity. If we consider only the 0−0 absorption band and assume a Gaussian band shape, the dipole strength $|\vec{\mu}|^2$ is given by $9.778 \times 10^{-3}\epsilon_o W n f^{-2}\bar{\nu}_o^{-1}$ D^2.[78] Figure 12 shows plots of the dipole strength calculated using two different expressions for f. The Lorentz expression $f = (n^2 + 2)/3$, which has been used by Shipman[80] for chlorophyll-*a* and -*b*, models the molecule as a spherical virtual cavity in the solvent, while the cavity-field expression $f = 3n^2/(2n^2 + 1)$ pertains to an actual spherical cavity.[81] A model based on a virtual elipsoidal cavity might be more appropriate. However, the values of the dipole strength calculated using the cavity-field expression are essentially independent of n, suggesting that this treatment corrects reasonably well for solvent effects in the particular case of BChl-*a* (see Figure 12). The mean value of $|\vec{\mu}|^2$ is 39.9 ± 0.3 D^2. By contrast, the values obtained using the Lorentz correction decrease systematically with n. This dependence is not removed by excluding H-bonding solvents.

The dipole strengths calculated in this way neglect a broad vibrational shoulder on the blue side of the absorption band. From spectra presented by Becker et al.,[82] we calculate that including the vibrational structure up to 2000 cm^{-1} above the peak increases the calculated dipole strength to 51.3 D^2 in methanol (where the 0−0 band is relatively broad) and to 52.8 D^2 in pyridine (where the 0−0 band is relatively sharp).

Scherz and Parson[23] measured a dipole strength of 41 D^2 for the Q_y band of BChl-*a* in acetone (including the vibrational shoulder) and 13 D^2 for the Q_x band (including only the 0−0 band). These values were obtained with the Lorentz correction factor. Using the cavity-field factor increases them to 48 and 15 D^2, respectively. Including the vibrational structure would increase the Q_x dipole strength to approximately 19 D^2.

Supporting Information Available: Molecular orbital expansion coefficients and CI coefficients for BChl in the three geometries found in the LH2 crystal structure (4 pages). Ordering information is given on any current masthead page.

References and Notes

(1) van Grondelle, R.; Dekker, J. P.; Gilbro, T.; Sundström, V. *Biochim. Biophys. Acta* **1994**, *1187*, 1−65.

(2) Freer, A.; Prince, S.; Sauer, K.; Papiz, M.; Hawthornthwaite-Lawless, A. M.; McDermott, G.; Cogdell, R. J. *Structure* **1996**, *4*, 449−461.

(3) Papiz, M. Z.; Prince, S. M.; Hawthornthwaite-Lawless, A. M.; McDermott, G.; Freer, A. A.; Isaacs, N. W.; Cogdell, R. J. *Trends Plant Sci.* **1996**, *1*, 198−206.

(4) McDermott, G.; Prince, S. M.; Freer, A. A.; Hawthornthwarte-Lawless, A. M.; Papiz, M. Z.; Cogdell, R. J.; Isaacs, N. W. *Nature* **1995**, *374*, 517−521.

(5) Koepke, J.; Hu, X.; Muenke, C.; Schulten, K.; Michel, H. *Structure* (*London*) **1996**, *4*, 581−597.

(6) Wu, H.-M.; Reddy, N. R. S.; Small, G. J. *J. Phys. Chem.* **1997**, *101*, 651−656.

(7) Sauer, K.; Cogdell, R. J.; Prince, S. M.; Freer, A. A.; Isaacs, N. W.; Scheer, H. *Photochem. Photobiol.* **1996**, *64*, 564−576.

(8) Breton, J.; Verméglio, A.; Garrigos, M.; Paillotin, G. In *Photosynthesis III. Structure and Molecular Organization of the Photosynthetic Apparatus*; Akoyunoglu, G., Ed.; Balaban International Science Services: Philadelphia, PA, 1981; pp 445−459.

(9) Angerhofer, A.; Bornhauser, F.; Gall, A.; Cogdell, R. J. *Chem. Phys.* **1995**,*194*, 259−274.

(10) Shreve, A. P.; Trautmann, J. K.; Frank, H. A.; Owens, T. G.; Albrecht, A. C. *Biochim. Biophys. Acta* **1991**, *1058*, 280−287.

(11) Hess, S.; Visscher, K. J.; Pulleritis, T.; Sundström, V.; Fowler, G. J. S.; Hunter, C. N. *Biochemistry* **1995**, *35*, 8300−8305.

(12) Jimenez, R.; Dikshit, S. N.; Bradforth, S. E.; Fleming, G. R. *J. Phys. Chem.* **1996**, *100*, 63−73.

(13) Warshel, A. *Comput. Chem.* **1977**, *1*, 195−202.

(14) Warshel, A.; Lappicirella, V. A. *J. Am. Chem. Soc.* **1981**, *103*, 4664−4673.

(15) Warshel, A.; Parson, W. W. *J. Am. Chem. Soc.* **1987**,*109*, 6143−6152.

(16) Parson, W. W.; Warshel, A. *J. Am. Chem. Soc.* **1987**, *109*, 6152−6163.

(17) Parson, W. W.; Breton, J.; Nabedryk, E. *Biochemistry* **1992**, *31*, 7503−7510.

(18) Parson, W. W.; Creighton, S.; Warshel, A. *J. Am. Chem. Soc.* **1989**, *111*, 4277−4284.

(19) Gouterman, M. *J. Mol. Spectrosc.* **1961**, *6*, 138−163.

(20) Petke, J. D.; Maggoira, G. M.; Shipman, L. L.; Christofferson, R. E. *Photochem. Photobiol.* **1980**, *32*, 399−414.

(21) Jentzen, W.; Simpson, M. C.; Hobbs, J. D.; Song, X.; Ema, T.; Nelson, N. Y.; Medforth, C. J.; Smith, K. M.; Veyrat, M.; Mezzanti, M.; Ramasseul, R.; Marchon, J. L.; Takenuchi, T.; Goddard, W. A., III; Shelnutt, J. A. *J. Am. Chem. Soc.* **1995**, *117*, 11085−11097.

(22) Barkigia, K. M.; Chantranupong, L.; Smith, K. M.; Fajer, J. *J. Am. Chem. Soc.* **1988**, *110*, 7566−67.

(23) Scherz, A.; Parson, W. W. *Biochim. Biophys. Acta* **1984**, *766*, 653−665.

(24) Roothaan, C. C. J. *J. Chem. Phys.* **1951**, *19*, 1445−1458.

(25) Warshel, A.; Russell, S. T.; Churg, A. K. *Proc. Natl. Acad. Sci. U.S.A.* **1984**, *81*, 4785−4789.

(26) Murrell, J. N.; Tanaka, J. *J. Mol. Phys.* **1964**, *7*, 363−380.

(27) Azumi, T.; Armstrong, A. T.; McGlynn, S. P. *J. Chem. Phys.* **1964**, *41*, 3839.

(28) Warshel, A.; Creighton, S.; Parson, W. W. *J. Phys. Chem.* **1988**, *92*, 2696−2701.

(29) Plato, M.; Mobius, K.; Michel-Beyerle, M. E.; Bixon, M.; Jortner, J. *J. Am. Chem. Soc.* **1988**, *110*, 7279−7285.

(30) Scherer, P. O. J.; Fischer, S. F. *Chem. Phys. Lett.* **1987**, *103*, 32−36.

(31) Warshel, A.; Parson, W. W. *Annu. Rev. Phys. Chem.* **1991**, *42*, 279−309.

(32) Moser, C. C.; Keske, J. M.; Warncke, K.; Farid, R. S.; Dutton, P. L. *Nature* **1992**, *355*, 796−802.

(33) Tinoco, I. *Adv. Chem. Phys.* **1962**, *4*, 113−159.

(34) Hayes, J. M.; Gillie, J. K.; Tang, D.; Small, G. J. *Biochim. Biophys. Acta* **1988**, *932*, 287−305.

(35) Reddy, N. R. S.; Picorel, R.; Small, G. J. *J. Phys. Chem.* **1992**, *96*, 6458−6464.
(36) Reddy, N. R. S.; Cogdell, R. J.; Zhao, L.; Small, G. J. *Photochem. Photobiol.* **1993**, *57*, 35−39.
(37) Manneback, C. *Physica* **1951**, *17*, 1001−1010.
(38) Cogdell, R. J.; Durant, I.; Valentine, J.; Lindsay, J. G.; Schmidt, K. *Biochim. Biophys. Acta* **1983**, *722*, 427−455.
(39) Clayton, R. K. *Photochem. Photobiol.* **1966**, *5*, 669−677.
(40) Cogdell, R. J.; Scheer, H. *Photochem. Photobiol.* **1985**, *42*, 669−689.
(41) Angerhofer, A.; Cogdell, R. J.; Hipkins, M. F. *Biochim. Biophys. Acta* **1986**, *848*, 333−341.
(42) Sturgis, J. N.; Hunter, C. N.; Niederman, R. A. *Photochem. Photobiol.* **1988**, *48*, 243−247.
(43) Pullerits, T.; Chachisvilis, M.; Sundström, V. *J. Phys. Chem.* **1996**, *100*, 10787−10792.
(44) Novoderezhkin, V. I.; Razjivin, A. P. *FEBS Lett.* **1993**, *330*, 5−7.
(45) Novoderezhkin, V. I.; Razjivin, A. P. *Biophys. J.* **1995**, *68*, 1089−1100.
(46) Bradforth, S. E.; Jimenez, R.; Van Mourik, F.; Van Grondelle, R.; Fleming, G. R. *J. Phys. Chem.* **1995**, *99*, 16179−16191.
(47) Neinhaus, G. U.; Mourant, J. R.; Chu, K.; Frauenfelder, H. *Biochemistry* **1994**, *33*, 13413−13430.
(48) Wu, H.-M.; Savikhin, S.; Reddy, N. R. S.; Jankowiak, R.; Cogdell, R.; Struve, W. S.; Small, G. J. *J. Phys. Chem.* **1996**, *100*, 12022−12033.
(49) Van Amerongen, H.; Van Haeringen, B.; Van Gurp, M.; Van Grondelle, R. *Biophys. J.* **1991**, *59*, 992−1001.
(50) Kramer, H. J. M.; Van Grondelle, R.; Hunter, C. N.; Westerhuis, W. H. J.; Amesz, J. *Biochim. Biophys. Acta* **1984**, *765*, 156−165.
(51) Nagarajan, V.; Alden, R. G.; Williams, J. C.; Parson., W. W. *Proc. Natl. Acad. Sci. U.S.A.* **1996**, *93*, 13774−13779.
(52) Renge, I.; Mauring, K.; Avarmaa, R. *J. Lumin.* **1987**, *37*, 207−214.
(53) Lathrop, E. J. P.; Friesner, R. A. *J. Phys. Chem.* **1994**, *98*, 3050−3055.
(54) Woodbury, N. W. T.; Parson, W. W. *Biochim. Biophys. Acta* **1984**, *767*, 345−361.
(55) Simpson, W. T.; Peterson, D. L. *J. Chem. Phys.* **1957**, *26*, 588−593.
(56) Förster, T. In *Modern Quantum Chemistry*; Sinanoglu, O., Ed.; Academic Press: New York, 1966; Part III, pp 93−137.
(57) Connolly, J. S.; Samuel, E. B.; Janzen, A. E. *Photochem. Photobiol.* **1982**, *36*, 565−574.
(58) Fidder, H.; Knoester, J.; Wiersma, D. A. *J. Chem. Phys.* **1991**, *95*, 7880−7088.
(59) Gudowska-Nowak, E.; Newton, M. D.; Fajer, J. *J. Phys. Chem.* **1990**, *94*, 5795−5801.
(60) Thompson, M. A.; Zerner, M. C.; Fajer, J. *J. Phys. Chem.* **1991**, *95*, 5693−5700.
(61) Sturgis, J. N.; Hagemann, G.; Tadros, M. H.; Robert, B. *Biochemistry* **1995**, *34*, 517−523.
(62) Sturgis, J. N.; Robert, B. *Photosynth. Res.* **1996**, *50*, 5−10.
(63) Hess, S.; Åkesson, E.; Cogdell, R. J.; Pullerits, T.; Sundström, V. *Biophys. J.* **1995**, *69*, 2211−2225.
(64) Hess, S.; Chachisvilis, M.; Timpmann, K.; Jones, M. R.; Fowler, G. J. S.; Hunter, C. N.; Sundström, V. *Proc. Natl. Acad. Sci. U.S.A.* **1995**, *92*, 12333−12337.
(65) Monshouwer, R.; Van Grondelle, R. *Biochim. Biophys. Acta* **1996**, *1275*, 70−75.
(66) Savikhin, S.; Struve, W. S. *Chem. Phys.* **1996**, *210*, 91−100.
(67) Kennis, J. T. M.; Streltsov, A. M.; Aartsma, T. J.; Nozawa, T.; Amesz, J. *J. Phys. Chem.* **1996**, *100*, 2438−2442.
(68) Xiao, W.; Lin, S.; Taguchi, A. K. W.; Woodbury, N. W. *Biochemistry* **1994**, *33*, 8313−8322.
(69) Novoderezhkin, V. I.; Razjivin, A. P. *FEBS Lett.* **1995**, *368*, 370-372.
(70) Visser, H. M.; Somsen, O. J. G.; Van Mourik, F.; Lin, S.; Van Stokkum, H. M.; Van Grondelle, R. *Biophys. J.* **1995**, *69*, 1083−1099.
(71) Leegwater, J. A. *J. Phys. Chem.* **1996**, *100*, 14403−14409.
(72) Kumble, R.; Palese, S.; Visschers, R. W.; Dutton, P. L.; Hochstrasser, R. M. *Chem. Phys. Lett.* **1996**, *261*, 396−404.
(73) Feick, R.; Van Grondelle, R.; Rijgersberg, C. P.; Drews, G. *Biochim. Biophys. Acta* **1980**, *593*, 241−253.
(74) Sebban, P.; Robert, B.; Jolchine, G. *Photochem. Photobiol.* **1985**, *42*, 573−578.
(75) Gottfried, D. S.; Stocker, J. W.; Boxer, S. G. *Biochim. Biophys. Acta* **1991**, *1059*, 63−75.
(76) Mulliken, R. S.; Rieke, C. A.; Orloff, D.; Orloff, H. *J. Chem. Phys.* **1949**, *17*, 1248−1267.
(77) Král, M. *Collect. Czech. Chem. Commun.* **1970**, *35*, 1939−1948.
(78) Harada, N.; Nakanishi, K. *Circular Dichroic Spectroscopy: Exciton Coupling in Organic Stereochemistry*; University Science Books: Mill Valley, CA, 1983; pp 406−423.
(79) Miller, J.; Gerhauser, J. M.; Matsen, F. A. *Quantum Chemistry Integrals and Tables*; University of Texas Press: Austin, TX, 1959.
(80) Shipman, L. L. *Photochem. Photobiol.* **1977**, *26*, 287−292.
(81) Böttcher, C. J. F. *Theory of Electric Polarization, 2nd ed.*; Elsevier: Amsterdam, 1973; pp 74−81, 166−168.
(82) Becker, M.; Nagarajan, V.; Parson, W. W. *J. Am. Chem. Soc.* **1991**, *113*, 6840−6848.